Chemical Engineering Science 274 (2023) 118674

Contents lists available at ScienceDirect

Chemical Engineering Science

journal homepage: www.elsevier.com/locate/ces

High-temperature sulfur capture by a Mn-Mo sorbent: An investigation of regeneration conditions and SO_2 formation and prevention

Jianyu Ma [a,b], Mehdi Mahmoodinia [a], Kumar R. Rout [c,d], Edd A. Blekkan [a,*]

[a] Dept. of Chemical Engineering, Norwegian University of Science and Technology (NTNU), NO-7491 Trondheim, Norway
[b] Present address: BYD, 3009 BYD Road, Pingshan District, Shenzhan, China
[c] SINTEF Industry, NO-7465 Trondheim, Norway
[d] Present address: Eramet Norway AS, c/o SINTEF Industry, NO-7465 Trondheim, Norway

HIGHLIGHTS

- The regeneration of a supported Mn-Mo sorbent for high-temperature desulfurization was studied.
- The influence of regeneration temperature (400 – 800 °C) and oxygen concentration (0.21 – 21 %) was investigated.
- SO_2 forms during initial stages of H_2S sorption with O_2-regenerated sorbent.
- Two mechanisms contribute to SO_2 formation: sulfate decomposition and H_2S conversion via oxidation.
- O_2-H_2 regeneration can prevent SO_2 formation.

ARTICLE INFO

Article history:
Received 26 October 2022
Received in revised form 7 March 2023
Accepted 19 March 2023
Available online 23 March 2023

Keywords:
High-temperature desulfurization
Mn-Mo sorbent
Regeneration
SO_2 formation
Sulfur residue

ABSTRACT

The regeneration performance of a solid sorbent (alumina-supported 15Mn8Mo) for sulfur capture at high temperature has been studied. The regeneration of the sulfided sorbent was performed by oxidizing at different temperatures (400 – 800 °C) and O_2 concentrations (0.21 – 21 %). Temperature had a larger impact on the regeneration than O_2 concentration. An unwanted side reaction during sulfur capture is SO_2 formation. Two pathways to SO_2 formation were identified, either via sulfate formation and decomposition or via oxidation of H_2S. A new regeneration method which avoids SO_2 formation and achieves low residual H_2S level in the gas phase involves adding an extra H_2 pre-reduction step between the regular O_2 -regeneration and the subsequent sorption step, i.e., a O_2 – H_2 regeneration. The stability of the sorbent was verified by 10 repeated sorption/regeneration cycles, with the sorbent regenerated either via the oxidative method or the new O_2 – H_2 regeneration method.

1. Introduction

Syngas from biomass gasification is a crucial renewable intermediate for electric power generation and synthetic fuel production. However, the innate presence of undesired pollutants, such as particulate matter, tar, sulfur and nitrogen compounds in the raw biogas is a major hurdle in the commercialization of advanced gasification based technologies (Huber et al., 2006). Among these contaminants, sulfur species are the key components hampering the catalytic conversion of the syngas fuels and chemicals (Wu et al., 2018). A variety of sulfur containing compounds are found in raw biogas such as hydrogen sulfide (H_2S), carbonyl sulfide (COS), carbon disulfide (CS_2), and sulfur-containing organics. However, the concentration of H_2S is higher than that of any other sulfur compounds (Meng et al., 2010). The associated detrimental properties (catalyst poisoning, corrosion, etc.) of these chemical compounds damages the downstream process units, catalysts, and instruments. Therefore, the syngas must be virtually devoid of sulfur prior to downstream catalytic processes with sensitive transition metal catalysts such as the Fischer-Tropsch process or methanol synthesis (Woolcock and Brown, 2013; Lillebø et al., 2013; Abdoulmoumine et al., 2015). Compared to conventional cold gas cleaning technologies, typically involving scrubbing solutions, high-temperature desulfurization with metal oxide sorbents is projected to be more energy-efficient and simultaneously offers lower cost due to its higher operating temperature conditions. This reduces heat transfer needs and provides the opportunity for energy recovery (Meng et al., 2010; Cheah et al., 2009). This is a very important issue in biomass processes, since these processes

* Corresponding author.
E-mail address: edd.a.blekkan@ntnu.no (E.A. Blekkan).

https://doi.org/10.1016/j.ces.2023.118674
0009-2509/

often are designed for smaller scale of operation due to challenging feedstock supplies, hence process intensification and improvements are needed to compensate for the missing advantages of large-scale operations.

Westmoreland and Harrison proposed the high-temperature desulfurization (Westmoreland and Harrison, 1976). The main focus of their study was on the thermodynamics of the desulfurization performance of transition metals. Eleven promising candidates were reported: zinc, iron, manganese, molybdenum, vanadium, calcium, strontium, barium, cobalt, copper, and tungsten. The chemical reactions that can occur between the solid sorbents and the gas phase during the high-temperature desulfurization process are shown below:

$$M_xO_y(s) + xH_2S(g) + (y-x)H_2(g) \rightarrow xMS(s) + yH_2O(g) \quad (1)$$

$$MS(s) + H_2O(g) \rightarrow MO(s) + H_2S(g) \quad (2)$$

$$xMS(s) + \left(\frac{y}{2}\right)SO_2(g) \rightarrow M_xO_y(s) + \left(x + \frac{y}{2}\right)S(g) \quad (3)$$

$$xMS(s) + \left(\frac{y}{2}\right)O_2(g) \rightarrow M_xO_y(s) + xSO_2(g) \quad (4)$$

$$MS(s) + 2O_2(g) \rightarrow MSO_4(s) \quad (5)$$

where M represents metals. H_2S is removed from the gas phase by reaction with metal oxides through reaction (1). The spent sorbent, with all or much of the metal in the form of metal sulfide can be regenerated with different oxidizing agents through different pathways (Reactions 2–4). Sulfate formation (Reaction (5)) is undesired as the sulfate is difficult to decompose and leads to sorbent deactivation (Cheah et al., 2009).

Manganese (Mn)-oxide provides a high initial reaction rate with H_2S in the temperature range of 327–827 °C (Westmoreland and Harrison, 1976). Furthermore, Mn oxide cannot be easily reduced to metallic Mn at temperatures lower than around 1650 °C (Gasper-Galvin et al., 1998), whereas this is a severe problem for zinc- and copper oxides if they are used as desulfurization solid sorbents at temperatures higher than 400 °C (Meng et al., 2010). Hence, Mn-based solid sorbents have been studied extensively, in the forms of single or mixed oxides (Ben-Slimane and Hepworth, 1994; Hepworth, 1994), considering the role of different supports (Chytil et al., 2017), and promoters (Yasyerli, 2008; Zhang et al., 2003; Karayilan et al., 2005). In our previous work, a series of Mn-based solid sorbents with different molybdenum (Mo) additions, as the promoter, have been studied for the biogas desulfurization process (Ma et al., 2020). It was shown that Mo addition promotes the desulfurization performance of the Mn–based sorbent in terms of capacity and stability. Formation of the $MnMoO_4$ phase was suggested to play a major role in the promotion mechanism.

One of the crucial factors for a qualified desulfurization sorbent, based on the criteria proposed by Bakker et al. (Bakker et al., 2003), is the regeneration capability of the sorbent, where the sorbent is reverted to its oxide form. O_2 is commonly used as a regeneration agent for solid sorbents (Cheah et al., 2009), however because of the extremely exothermic oxidation reaction (Reaction (4)), controlling the O_2 concentration is critical to minimize sintering and consequent sorbent reactivity loss (Zeng et al., 1999). High O_2 concentration during the regeneration cycle might also promote the formation of manganese sulfate, $MnSO_4$, via reaction (5), which leads to sorbent deactivation (Cheah et al., 2009). It has been reported that applying a high temperature, i.e. 800 °C, can facilitate the conversion of $MnSO_4$ to Mn_3O_4 (Yu et al., 2010; Wang et al., 2016; Liu et al., 2016), however such a high temperature can also lead to sintering of the material. Therefore, optimizing both temperature and O_2 concentration are important factors during the regeneration step to retain good sorbent properties.

In this study, the role of the regeneration conditions on the sorbent performance was investigated using thermogravimetric analysis (TGA), supported by thermodynamic calculations. SO_2 formation during sorption from a syngas mixture has been predicted from thermodynamic calculations (see e.g. (Ma et al., 2020). SO_2 in a humid atmosphere can be corrosive, and importantly, the release of SO_2 during the initial phase of sorption (e.g. when a regenerated sorbent is brought back on-line) is undesired since this negates the cleaning effect of the sorbent. SO_2 can also react with H_2S and form elemental sulfur, potentially leading to fouling and plugging of the equipment. Hence, the mechanism of SO_2 formation was studied by combining the theoretical calculations and experimental results obtained from a fixed-bed reactor equipped with a dedicated sulfur analyzer capable of quantifying low gas-phase concentrations (ppb-range) and a quadrupole mass spectrometer (QMS) with a rapid response to changes in concentration. We propose two routes to SO_2 formation, either from H_2S oxidation by metal oxides or from metal sulfate decomposition. Finally, a new regeneration method is proposed to prevent SO_2 formation and improve the process of cleaning the raw biogas.

2. Experimental and methods

2.1. Chemicals

Manganese nitrate ($Mn(NO_3)_2{\cdot}4H_2O$) and ammonium molybdate ($(NH_4)_6Mo_7O_{24}{\cdot}4H_2O$) were used as received from Sigma Aldrich. Aluminium-oxide support γ-alumina LOT#B5160010 was obtained from Strem chemicals.

2.2. Sample preparation

A solid sorbent with Mn and Mo loading of 15 wt% and 8 wt% respectively (termed 15Mn8Mo), was prepared using γ-alumina support and the incipient wetness impregnation method. In a typical synthesis, the calculated amounts of metal pre-cursors (Mn, Mo) were completely dissolved in a predetermined volume of deionized water (corresponding to the pore volume of the support), where the as-prepared homogeneous solution was added dropwise to the γ-alumina support in a beaker. The resulting sorbent was then aged, dried for 12 h under 100 °C, and calcined at 650 °C for 5 h using a ramp rate of 10 °C/min. The calcined catalyst was crushed and sieved to obtain a particle size of 150–200 μm. More details about the synthesis procedure can be found in our previous study (Ma et al., 2020).

2.3. Instrumentation and methodologies

A Bruker AXS D8 Focus diffractometer equipped with CuKα radiation (λ = 0.154 nm) was used to acquire X-ray diffraction (XRD) patterns. The crystallite size was calculated using the Scherrer equation using a shape factor of 0.9. Textural properties of the sorbent (BET surface area and pore size) were obtained using a Micromeritics TriStar 3020 instrument using isothermal N_2 adsorption–desorption at −196 °C. The sorbent was degassed under vacuum at 200 °C for 8 h prior to the measurements. The X-ray photoelectron spectroscopy (XPS) was recorded on a Kratos Axis Ultra spectrometer equipped with a monochromatic Al K(alpha) source (100 W). The samples were mounted on a carbon tape prior to loading into the instrument loading chamber. The exposed analysis area was approximately 300 × 700 μm^2. A pass energy of 40 eV was used for core level regions. The acquired spectra have been charge-corrected to the mainline of the C 1 s spectrum (ad-

ventitious carbon), set to 284.8 eV, and fitted using Gaussian–Lorentzian functions implemented in the CasaXPS software, version (2.3.23), after subtracting a Shirley/Linear background.

2.3.1 *Performance tests:* The chemical looping desulfurization tests were conducted in a laboratory setup consisting of a gas supply and regulation system, a tubular fixed-bed reactor, and gas analyzing modules. The schematic diagram of the desulfurization setup is shown in Fig. S1. Further details describing the experimental procedure can be found in our previous work (Ma et al., 2020). During the desulfurization tests, 0.2 g of the 15Mn8Mo/Alumina sorbent (the composition with the best desulfurization performance in our previous study (Ma et al., 2020) was loaded in the reactor and heated up to 600 °C with a ramping rate of 10 °C/min, and held in an H_2/N_2 gas mixture (50 mL/min with 50 vol% H_2) for 1 h. Following this pretreatment, the model biogas was first introduced into a bypass line connected to the QMS for 25 min to stabilize the spectrometer signal, and then the gas flow was switched into the reactor where the sorption occurs in a fixed bed mode. The exhaust gas from the reactor is directed to the QMS for analysis. The sorption step was conducted with a model syngas composition with 0.4, 39.6, 40.0, and 20 vol% of H_2S, Ar, H_2, and N_2, respectively, and a total flow rate of 100 mL/min. The sorption step was stopped when the H_2S breakthrough was observed, here defined as when the H_2S outlet concentration was 40 ppm above the lowest observed level. The sorbent regeneration step was conducted at the same temperature, 600 °C, using a gas mixture of 25 vol% of air diluted with N_2 with the flow rate 100 mL/min. After each sorption and regeneration steps the system was flushed with 100 mL/min N_2 for 10 min. The desulfurization tests were conducted with 10 repeated sorption-regeneration cycles. In addition, a novel regeneration method was carried out by introducing a pre-reduction step following the regeneration step by feeding a gas mixture of H_2/N_2 (100 mL/min with 50 % H_2) for 10 min at 600 °C. The complete protocol for the performance tests contained sequential sorption, regeneration, and reduction steps of the sorbent.

The outlet gas composition was analyzed continuously by a ThermoStar GSD 320 T1 C analytical system equipped with a quadrupole mass spectrometer (QMS 200) using a secondary electron multiplier detector. The quantitative results were based on a regular calibration of the spectrometer responses, and the desulfurization capacity was calculated based on the measured concentration curves. The breakthrough capacity (*BC*) was utilized and calculated as follows:

$$BC\left(\frac{g\ of\ H_2S}{g\ of\ sorbent}\right) = \frac{Q \times \int_0^t (c_{in} - c_{out}) \times M_{H_2S}}{24.04 \times 10^9 \times m_s} \quad (6)$$

where Q is the flow rate of the gas mixture, i.e., 100 mL/min; C_{in} and C_{out} are the inlet and outlet concentration of H_2S (ppm); m_s is the mass of the loaded solid sorbent, typically 0.2 g, and M_{H_2S} is the molecular weight of H_2S.

2.3.2 *Lowest level (residual gas phase sulfur) tests:* A dedicated sulfur analyzer, Thermo Fischer 450i, was utilized to precisely measure the residual H_2S and SO_2 concentrations in the cleaned biogas (the off gas from reactor during the sorption cycle) as the QMS has limited sensitivity to very low concentrations. The sulfur analyzer applies a pulsed fluorescence technology, where the sulfur-containing molecules are exited using UV-light, and the intensity of the light emitted during relaxation is measured. A lower H_2S concentration (i.e., 0.2 vol%), compared to that of the regular performance tests (0.4 vol%), was chosen to conduct the lowest level tests to ensure that the breakthrough time is long enough for obtaining enough measurement points and that the sulfur concentration has not surpassed the upper detection limit of the instrument. Like the regular performance test, the feed gas mixture was first stabilized through the bypass line for 25 min, and then switched to the sorption reactor. The off gas from the reactor was initially monitored using the QMS for one minute to ensure that the H_2S concentration in the exhaust gas reached a low and stable level below the upper detection limit of the sulfur analyzer (<10 ppm), then it was diluted with synthetic air by a factor of 5 before switching to the analyzer. The H_2S and SO_2 concentrations were measured with one-minute intervals and corrected for the dilution by following equation.

$$RC_s(ppm) = 5 \times RC_D \quad (7)$$

where RC_s is the concentration of H_2S or SO_2 in the off-gas, and RC_D is the measured value in the diluted gas stream.

2.3.3 *Regeneration conditions:* The impacts of regeneration temperature and oxygen concentration on the sorbent performance were carried out in a thermogravimetry (TGA) instrument, Linseis STA PT1600. A fully sulfided sorbent (also called 15Mn8Mo-AS), i.e., the sulfidation cycle was well beyond the breakthrough curve from the QMS signal, was utilized to conduct such studies. Approx. 15 mg of the sulfided sorbent was heated up to certain temperatures, i.e. 400 °C, 600 °C or 800 °C, with a ramping rate of 10 °C/min, under a purge flow of 200 mL/min Ar, followed by 30 min stabilization at the chosen temperature. The sample was then regenerated under diluted air/Ar with different air concentrations (i.e. 1 %, 10 %, or 100 %), for 15 min, followed by a cooling-down step to room temperature under Ar purge. These samples were subsequently analyzed by XRD. The regenerated samples were labeled as 15Mn8Mo-AR with the corresponding conditions, for example, a sample regenerated at 600 °C and using 100 % air was named 15Mn8Mo-AR-T600-100 %.

2.4. Thermodynamic analysis

Thermodynamic calculations were performed using the Phase module implemented in the Factsage 7.0 software (Bale et al., 2016). The predominant phase diagram for Mn—S—O and Mo—S—O systems were calculated under different temperatures and O_2 partial pressures, $p(O_2)$, to provide a guideline to design and validate the regeneration process (Fig. 1). A temperature range of 200 – 1000 °C, and a $p(O_2)$ range of 10^{-16} to 1 atm were used in the calculations, while keeping the total pressure at 1 atm. The ratio between mole fractions of Mn and S was set to 1, corresponding to MnS, and the ratio of Mo and S was set to 2, as for MoS_2. $MnSO_4$ is the dominant phase at T < 600 °C, according to the Mn—S—O phase diagram (Fig. 1A), even at very low $p(O_2)$, and therefore, a higher temperature is required to avoid sulfate formation. In pure air ($p(O_2) = 0.21$atm), a temperature higher than 900 °C is required to regenerate Mn as Mn_2O_3 while avoiding sulfate formation. MnS is the dominant phase at T > 600 °C and at extremely low partial pressure of O_2 and cannot be regenerated even at very high temperatures.

As shown in the Mo—S—O phase diagram in Fig. 1B, formation of molybdenum sulfate is thermodynamically not feasible within the calculation range. At higher $p(O_2)$, and T > 830 °C, the dominant phase is MoO_3, and by decreasing the $p(O_2)$, , a mixture of Mo oxides could form. Similar to MnS formation in Fig. 1A, MoS is the dominant phase at T > 600 °C and at extremely low $p(O_2)$ (Fig. 1B).

The theoretical values for gas-phase residual H_2S concentration and conversion to SO_2 over Mn- and Mo-oxides as a function of temperature are presented in Fig. 2A and 2B, respectively. The model gas mixture used in these calculations is the same as that used in our desulfurization experiments. The residual H_2S concentrations increases with increasing temperature for all modeled metal oxides, as shown in Fig. 2A, with Mn_3O_4 having the highest residual H_2S (i.e., over 100 ppm at T > 500 °C), followed by MoO_2 and MnO. The residual H_2S concentrations over MoO_2 and MnO

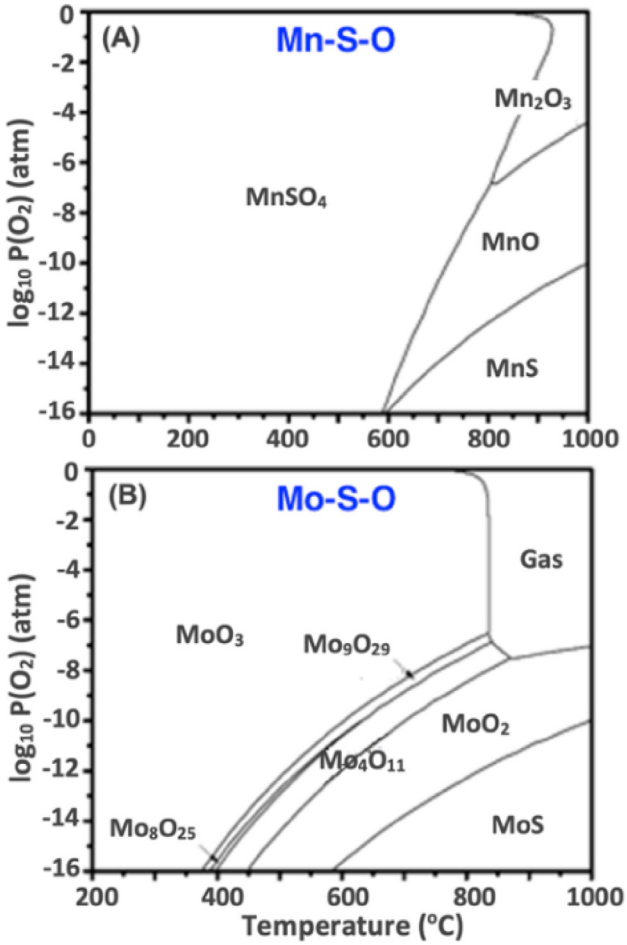

Fig. 1. Predominant phase diagram for (A) Mn—S—O and (B) Mo—S—O systems at various $p(O_2)$ as a function of temperature.

surpass 1 ppm at T > 480 °C and T > 550 °C, respectively. The lowest H_2S residual level is seen with Mn_2O_3 and MoO_3.

The residual SO_2 level is virtually insignificant in the presence of Mn_3O_4, MnO, and MoO_2, indicating that there is almost no H_2S to SO_2 conversion, as shown in Fig. 2B. However, in the presence of Mn_2O_3 at T > 450 °C and in the presence of MoO_3 across the entire temperature range, nearly all H_2S is converted to SO_2. Hence, the thermodynamic analysis suggests that metal oxides with the lowest oxidation states, such as MnO and MoO_2, are the most suitable oxides for H_2S capture at temperatures higher than 600 °C.

3. Results and discussion

3.1. Effects of regeneration temperature and O_2 concentration

The thermodynamic calculations show that the system favors low oxidation states of metal oxides for effective combined desulfurization, that is, to remove both H_2S from the gas and avoid the formation of SO_2. Additionally, the sorbent capacity must be maintained by minimizing metal sulfate formation (Cheah et al., 2009). As shown in the phase diagrams above, partial pressure of oxygen and temperature are important parameters for metal sulfate formation. This emphasizes the critical role of the regeneration step in maintaining sorbent performance during successive/alternative sorption cycles. Therefore, the primary goal is to regenerate the metal sulfide to a lower oxidation state metal oxide while preventing the formation of metal sulfate.

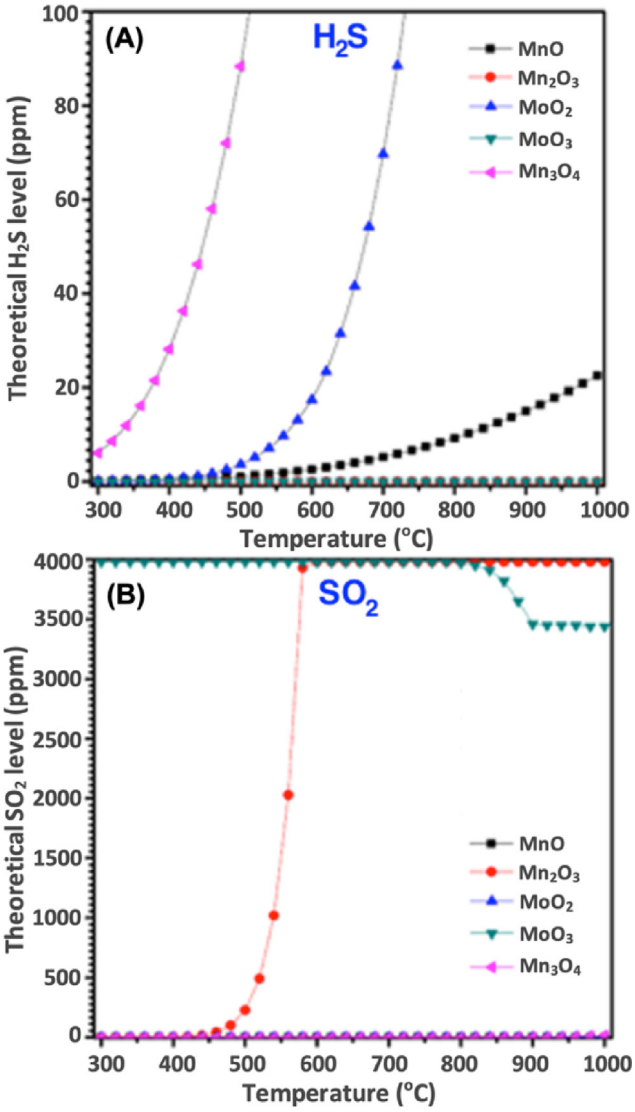

Fig. 2. Theoretical values for equilibrium concentration of (a) H_2S and (b) SO_2 on different metal oxides as a function of temperature.

TGA was employed in this work to explore the impact of the aforementioned parameters on the performance of 15Mn8Mo solid sorbent. Different ranges of regeneration temperatures (i.e., 400 °C, 600 °C, and 800 °C) and oxygen concentrations (i.e., 1 vol%, 10 vol%, and 100 vol% air representing 0.21 vol%, 2.1 vol% and 21 vol% O_2 concentrations, respectively) were tested.

Fig. 3A shows the associated XRD patterns of fresh and sulfided sorbents. The $MnMoO_4$ phase, which is a mixture of MnO and MoO_3 oxides, is the dominant crystallite phase in the fresh sorbent, in addition to the Al_2O_3 phase. The sulfided sorbent, however, displayed prominent peaks at $2\theta = 30°$, 34.5°, 49.5°, 59°, and 67°, corresponding to the MnS phase, which is formed via reaction (1). The relatively small peak at 33° might represent the remaining Mn_2O_3 phase from fresh sorbent. Mo oxide and sulfided phases were absent in the XRD pattern of the spent sorbent. We cannot rule out the existence of such phases due to the limited sensitivity, especially for very small (below 3–4 nm) particles.

Diffraction patterns for the sorbents regenerated at varying temperature and gas mixtures are illustrated in Fig. 3B-3D. These XRD patterns show similar characteristic peaks irrespective of O_2 concentrations at each tested regeneration temperature. In contrast, dissimilarities between the XRD patterns arise when differ-

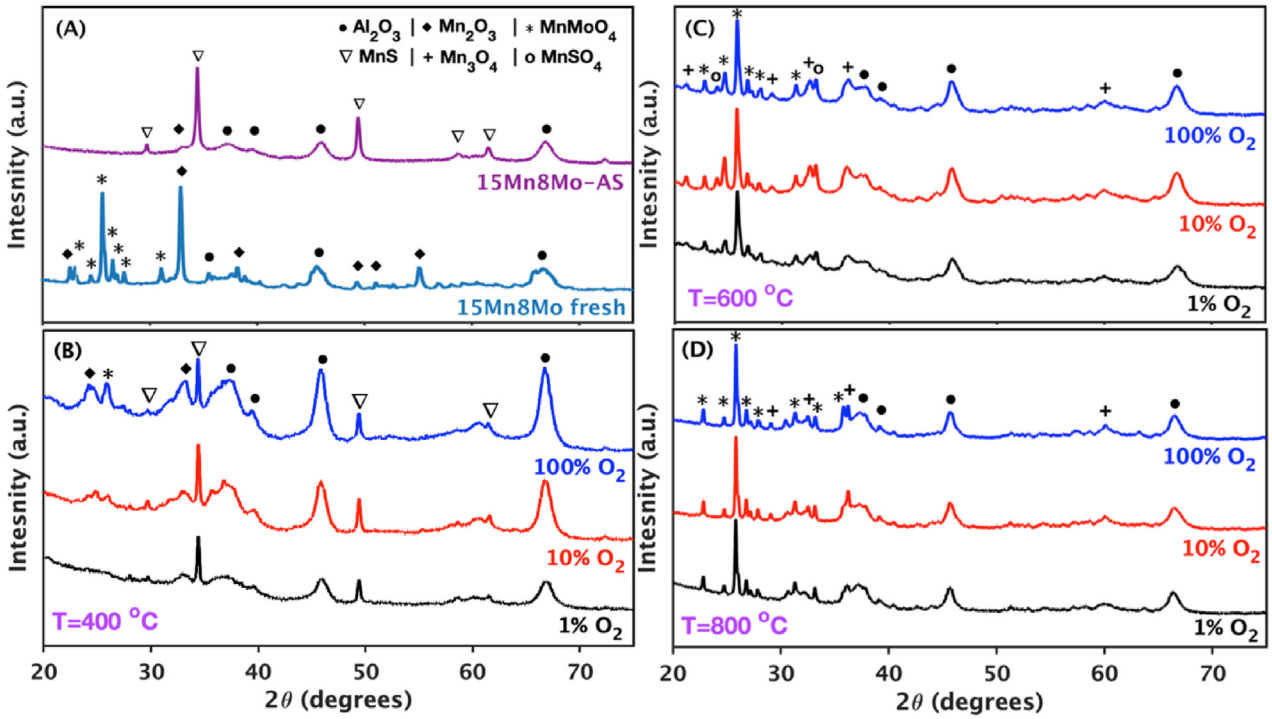

Fig. 3. XRD patterns of (a) fresh (15Mn8Mo) and sulfided (15Mn8Mo-AS) samples; regenerated samples (in TGA) in various O_2 concentrations at (b) 400 °C; (c) 600 °C; and (d) 800 °C.

ent regeneration temperatures are applied. This shows that the regeneration temperature has a dominant influence on the degree of regeneration compared to the O_2 concentration. Fig. 3B displays the diffraction pattern of the regenerated sorbent at 400 °C. The characteristic peaks at 2 θ values of 34° and 49°, attributed to MnS phase, indicate that regeneration was incomplete at 400 °C. However, with increased $p(O_2)$, the peaks corresponding to Mn_2O_3 and $MnMoO_4$ become more prominent. The MnS peak, on the other hand, shows an inverse relationship with $p(O_2)$ in the gas mixture. In other words, with higher $p(O_2)$ a complete regeneration should also be possible at 400 °C.

In all three samples that were regenerated at varying $p(O_2)$, the characteristic lines for MnS disappeared as the regeneration temperature was increased to 600 °C, and the samples display characteristic patterns of γ-alumina, Mn_3O_4, and $MnMoO_4$, (Fig. 3C). The characteristic peaks for the $MnMoO_4$ phase are clearer at 600 °C, even at low $p(O_2)$, compared to sorbents regenerated at 400 °C. It is however evident that the characteristic lines for $MnSO_4$ (2 θ values of 24° and 33.5°) are clearer at higher $p(O_2)$. This indicates that major fractions of MnS are converted to $MnSO_4$ in the presence of higher $p(O_2)$, which may cause an unavoidable drop in the sorbent capacity in the subsequent sorption step (Cheah et al., 2009). The progressive increase in the diffraction-lines representing the $MnMoO_4$ phase was maintained as the temperature increased from 400 °C to 600 °C and 800 °C. Importantly, sorbent regeneration at 800 °C left no evidence of the $MnSO_4$ phase at all tested O_2 concentrations. This observation is in agreement with our findings from thermodynamic calculations. Therefore, higher regeneration temperatures can either limit the formation of $MnSO_4$ phase or facilitate its decomposition.

The crystallite sizes of the active phases on the fresh and regenerated samples are evaluated by the Scherrer equation and the results are presented in Table 1. The peaks at 2θ values of 26°, 33°, and 29° were selected for calculating the crystallite sizes of $MnMoO_4$, Mn_2O_3, and Mn_3O_4 phases, respectively. Only the samples regenerated at 600 and 800 °C were evaluated since the regeneration at 400 °C was not completed as the leftover metal sulfide prevailed (Fig. 3B). The crystallite sizes of manganese oxide (Mn_2O_3) and $MnMoO_4$ phases on the fresh sample are calculated to 31 nm and 40 nm, respectively. The regeneration at 800 °C resulted in larger crystallite sizes for both manganese oxides (Mn_3O_4) and $MnMoO_4$ compared to those estimated at 600 °C. The impact of O_2 concentrations, on the other hand, is smaller. An increasing in O_2 concentration at 600 °C and 800 °C resulted in an increase in the crystallite sizes of $MnMoO_4$. Higher $p(O_2)$, on the other hand, resulted in a decrease in the crystallite sizes of manganese oxides (Mn_3O_4) at 600 °C, but an increase was observed at 800 °C. It is reported that both temperature and oxygen concentration have a large impact on sintering (Cheah et al., 2009). Our findings suggest that the regeneration temperature is far more detrimental than the O_2 concentration for sintering of the active phases. Therefore, the operating temperature for sorbent regeneration must be carefully selected for an optimal removal of captured sulfur and minimal sintering.

Table 1
Calculated crystallize sizes (by Scherrer equation) of different phases present on the fresh and regenerated samples in various O_2 concentrations at 600 °C and 800 °C.

Sorbent	Crystallite Size (nm)		
	Mn_3O_4	$MnMoO_4$	Mn_2O_3
fresh	–	40	31
600–1 %	38	39	–
600–10 %	35	42	–
600–100 %	28	46	–
800–1 %	69	59	–
800–10 %	54	62	–
800–100 %	72	57	–

3.2. Performance test with pre-reduction

Our thermodynamic calculations and experimental observations revealed that a higher temperature and higher O_2 concentra-

tions with longer regeneration times are beneficial for the complete elimination of sulfur during the regeneration step. We also found that high temperature led to sintering of active phases whereas lower temperature is inadequate to completely remove the sulfide phase. Hence, it is crucial to select optimal conditions for the regeneration step to not only maintain the active phases at low oxidation states (i.e., MnO and MoO_2), but also to avoid detrimental sulfate formation. Higher oxidation states of Mn (i.e., Mn_2O_3) could subsequently result in the formation of SO_2 in the subsequent sorption step (Fig. 2B).

3.2.1 Pre-reduction step: We investigated the effect of a pre–reduction step with H_2 for the spent sorbent in-between the regular O_2–regeneration and the next sorption step (a procedure we term O_2 –H_2 regeneration). The pre–reduction and regeneration temperatures were selected to be the same as the sorption temperature, 600 °C, and thus easy and economical to operate, moreover, less likely to result in sintering. Fig. S2 displays the recorded signals from QMS for H_2, H_2S, H_2O, N_2, and SO_2 throughout the desulfurization experiments. The presence of SO_2 is evident at the initial stage of sorption step for a sample that has been treated under regular O_2 regeneration (i.e., with no H_2 pre–reduction) at 600 °C (Fig. S2(A)). The stabilized feed gas was introduced into the reactor at t_0 and a rapid decline in H_2S concentration was observed. Simultaneously, a surge in concentration of SO_2 and H_2O was noticed. However, the former declined to a lower level after approx. 2 min whereas, the latter took approx. 8 min. Fig. S2(B) and S2(C) illustrate the changes in gas composition during a regular O_2 regeneration and the pre-reduction step, respectively. A broad SO_2 signal during the O_2 regeneration (Fig. S2(B)) is visible, which is ascribed due to chemical interaction between metal sulfide and O_2 (reaction (4)). Similarly, a sharp SO_2 peak, accompanied by a H_2O signal, is also visible at the early stage of the pre-reduction step, which fades away quickly after a few minutes. This and the SO_2 formation at the beginning of the sorption step (Fig. S2(A)) can be explained by the reaction between metal sulfate and H_2 (reaction (8)). (Xuan et al., 2020; Pishahang et al., 2016; Sjoerd Kijlstra et al., 1998)

Finally, Fig. S2 (D) reveals the importance of O_2 –H_2 regeneration steps, where no SO_2 signal is observed at the beginning of the next sorption. Therefore, the possibility to simultaneously avoid SO_2 formation and prevent H_2S oxidation by metal oxides during subsequent sorption cycle could be achieved by combining a regular O_2 regeneration step with a pre-reduction step using H_2. It should also be noted that the active metal oxides ($MnMoO_4$, Mn_3O_4) can undergo unwanted reduction as per reactions (9) and (10) during the pre-reduction step.

$$MnSO_4 + H_2 \rightarrow MnO + H_2O + SO_2 \quad (8)$$

$$Mn_3O_4 + H_2 \rightarrow 3MnO + H_2O \quad (9)$$

$$MnMoO_4 + H_2 \rightarrow MnO + MoO_2 + H_2O \quad (10)$$

From the perspective of practical applications, SO_2 formation during the initial part of the sorption step is detrimental to the overall operation of a biomass gasification and gas upgrading process. Elemental sulfur can be formed when H_2S interacts with SO_2 which leads to blockage or damage of downstream equipment (Xuan et al., 2020). Therefore, an additional pre-reduction step can eliminate the potential damage from SO_2 during H_2S removal in the subsequent sorption cycle.

3.3. SO_2 formation and prevention

Two routes for SO_2 formation during desulfurization process have been proposed, i.e., decomposition of metal sulfate in O_2 or H_2 atmosphere, and H_2S oxidation by metal oxides (Mn_2O_3, MnO_2) (Asaoka et al., 2012; Herszage et al., 2003) . The latter has already been observed experimentally during sorption and regeneration steps (Fig. S2) and this route is supported by our thermodynamic calculations (Fig. 2B). Davydov and co-worker also reported that Mn_2O_3 and MoO_3 are active for the oxidation of H_2S to SO_2, where Mn_2O_3 was the second most active catalyst among 21 tested candidates (Davydov et al., 2003).

To validate our hypotheses on the SO_2 formation routes, the 15Mn8Mo sorbent was pretreated in different ways, giving 5 different states of the material, before being used in sulfur residue tests at 600 °C. These states are (1) fresh (calcined) sorbent heated up and reduced with H_2 for 1 h (pretreatment similar to the performance tests); (2) fresh sorbent heated up under N_2 without reduction treatment; (3) sulfided sorbent regenerated with regular oxidation; (4) sulfided sorbent regenerated with regular oxidation and an extra H_2 treatment (O_2 –H_2 regeneration); (5) sulfided sorbent regenerated with regular oxidation and reduction, followed by an extra oxidation step (O_2 –H_2 –O_2 regeneration). The last test could shed light on the effect of higher oxidation states of metal oxides on SO_2 formation. In test (5) the O_2 – regenerated sample was treated with H_2 to remove the potential metal sulfates, and then re-oxidized again to oxides with higher oxidation states using the same conditions as in the O_2 regeneration for 10 min. Hence the sample was a mixture of Mn and Mo oxides, but sulfur free. Table 2 shows the dominant crystalline phases on all five samples, based on the XRD and TPR data and basic chemical understanding of these systems. (See also (Ma et al., 2021) for data on the single metal phases).

XPS analysis was employed to determine the oxidation state of Mo and Mn during the reduction, sulfidation, and regeneration process of samples 1–4 in Table 2. Fig. 4 displays the Mn 2p, Mo 3d, and S 2p core-level spectra of these samples. Both Mo and Mn tend to form various oxides with different oxidation states. Analysis of the XPS spectra of Mn 2p is even more challenging due to complex multiplet splitting, shake-up structure, and overlapping binding energy positions (Biesinger et al., 2011). The initial fitting parameters for Mn 2p components are based on the parameters presented in Table 2 of Biesinger et al. (Biesinger et al., 2011) for pure samples and then modified as needed for our mixed oxide samples. Fig. 4A shows the Mn 2p spectra with a 2p3/2 to 2p1/2 spin–orbit splitting of 11.3 eV. A shake-up satellite feature in the Mn 2p spectrum, at 645–648 eV, indicates the presence of Mn(II) in these samples (Di Castro and Polzonetti, 1989; Oku et al., 1975). The Mn 2p3/2 spectra corresponding to the Mn(II) and Mn (III) oxidation states presented in these samples are fitted with 6 and 5 peaks, respectively, due to multiplet splitting. In the fresh sample, Fig. 4A.I, the Mn(III) components are the dominant oxidation state of the Mn species with a relative concentration of ~ 62 %, and the rest corresponds to the Mn(II), in reasonable agreement with the findings from XRD analyses, Fig. 3A, indicating the presence of $MnMoO_4$ and Mn_2O_3 in this sample. For the reduced sample, Fig. 4A.II, the relative concentration of surface Mn(II) is increased substantially up to ~ 71 %, demonstrating the reduction

Table 2
List of the proposed dominant phases on the selected samples for sulfur residue tests at 600 °C.

Sample	Specifications	Dominant phases
1	fresh sorbent with H_2 treatment	MnO, MoO_2
2	fresh sorbent without H_2 treatment	Mn_2O_3, $MnMoO_4$
3	spent sorbent with O_2 regeneration	Mn_3O_4, $MnMoO_4$, $MnSO_4$
4	spent sorbent with O_2 –H_2 regeneration	MnO, MoO_2
5	spent sorbent with O_2 –H_2 –O_2 regeneration	Mn_3O_4, $MnMoO_4$

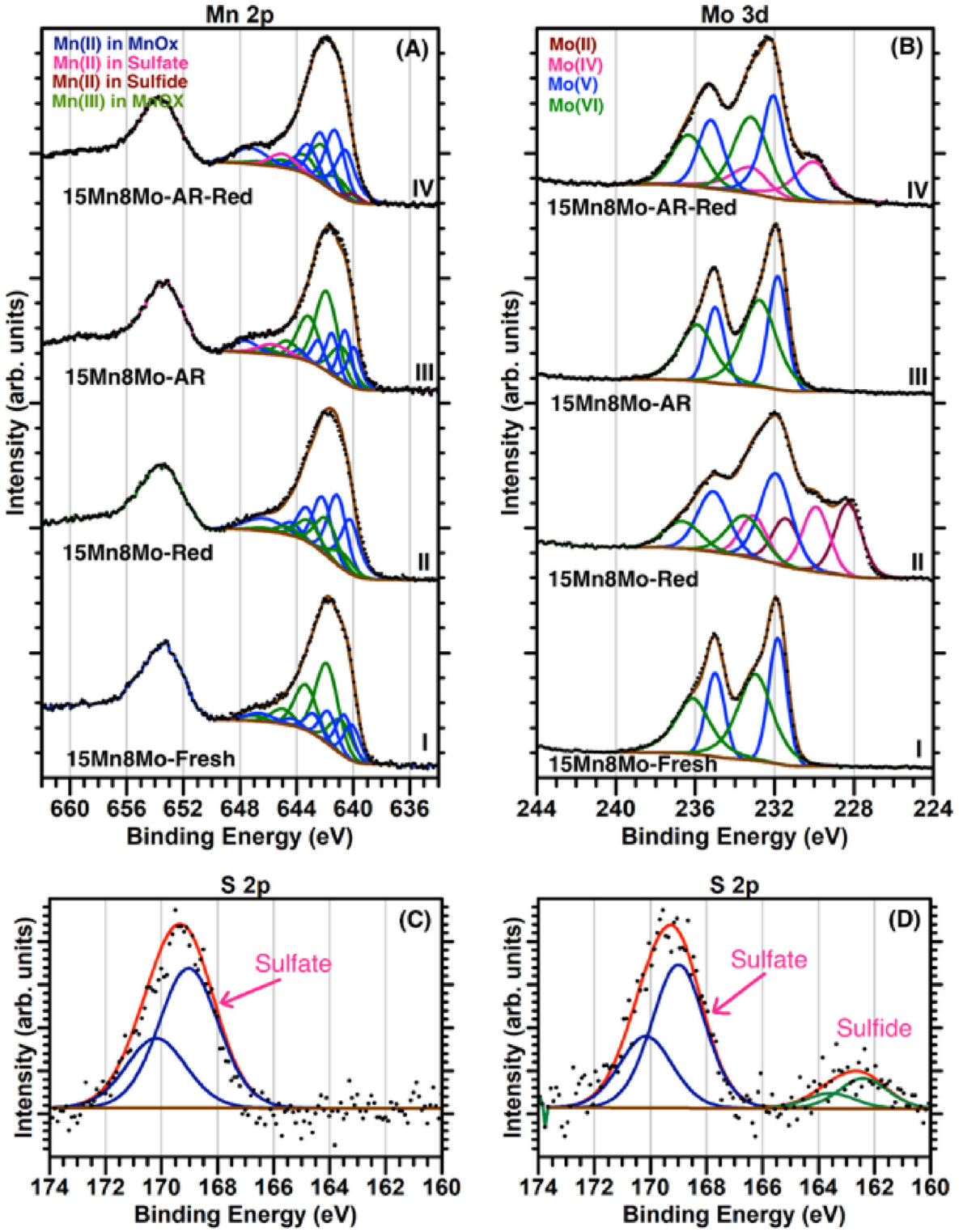

Fig. 4. XPS spectra of the energy regions of the sample 1– 4 listed in Table 2. (A) Mn 2p; (B) Mo 3d; (C): S 2p from spent sorbent with O_2 regeneration (sample 3); (D): S 2p from spent sorbent with O_2 –H_2 regeneration (sample 4).

of Mn_2O_3 to MnO during the reduction process. On the regenerated sample, Fig. 4A.III, the relative concentration of Mn(III) and Mn(II) returns to a similar level of fresh sample, however, a new peak emerges at 645.7 eV, corresponding to $MnSO_4$, suggesting that the side reaction (reaction (5)) may occur. The reducing treatment on the regenerated sample, Fig. 4A.IV converted most of the Mn(III) to Mn(II), and it also reduced some part of $MnSO_4$ to MnS. A small peak at ~ 640 eV binding energy confirms the presence of MnS in this sample. The presence of MnS and $MnSO_4$ is also clear from the S 2p core states at binding energies of 162.4 and 169 eV, respectively, in this sample (Fig. 4D). The S 2p XPS peak at 162.4 eV for MnS is, however, not detected for the regenerated sample (Fig. 4C). Conversion of sulfate to sulfide under H_2 treatment has been reported before (Xuan et al., 2018, 2020):

$$MnSO_4 + 4H_2 \rightarrow MnS + 4H_2O \quad (11)$$

$$2MnSO_4 + 5H_2 \rightarrow MnS + MnO + 5H_2O + SO_2 \quad (12)$$

Therefore, it seems harsher conditions are needed to completely remove the sulfur component from the regenerated solid sorbent.

The Mo 3d XPS spectra in Fig. 4B illustrate how the oxidation states of Mo in these samples change following various pretreatments. Mo 3d region also shows well separated spin–orbit components (Δ = 3.15 eV). The peak shape for the fresh (Fig. 4B.I) and regenerated (Fig. 4B.III) samples looks similar, and they are fitted by two spin–orbit doublets with peaks at binding energies of ~ 231.8 and ~ 233.0 eV, corresponding to the Mo(V) and Mo (VI) oxidation states, respectively. The XPS spectra for Mo(VI) correspond to the presence of $MnMoO_4$ species in these samples, which is also supported by XRD data (Fig. 3A). However, no phases with oxidation states of Mo(V) are detected under XRD. This might be due to the amorphous structure of these species, or their particle sizes are below the detection limit (lower than 3–4 nm) of the XRD instrument. Following the reduction treatment on either the fresh or regenerated sample, Mo with lower oxidation states emerged at lower binding energies of 229 and 228.3 eV for the Mo(IV) and Mo(II) states, respectively, which may be attributed to $MnMoO_4$ decomposition to MnO and MoO_3, and the subsequent reduction of MoO_3. It is worth mentioning that the reduction of the fresh sample is more severe than of the regenerated sample due to a longer reduction step. This can explain the presence of a lower oxidation state of Mo which we assigned to Mo(II) in Fig. 4B.II. However, Mo with higher oxidation states (V and VI) are still the dominant oxidation states in these samples.

3.4. Residual sulfur level tests and role of H_2 pre-reduction

The pretreated sorbents (Table 2) were subsequently utilized in sorption studies with the emphasis on gas-phase sulfur concentration (residue) measurements at 600 °C. The dedicated sulfur analyzer was used to quantify the residual H_2S and SO_2 concentrations in the cleaned gas with high precision (within a range of 10 ppm down to several ppb). The results for lowest attainable H_2S and SO_2 levels in the gas phase for all tested samples are shown in Fig. 5. Briefly, the observed H_2S concentration for all tested samples were initially high, then gradually decreased and attained a stable level. As described earlier, the sulfidation experiment starts with a stabilization step through a by-pass line, followed by the sorption experiment by switching the gas flow to the reactor line. Hence, the initial H_2S peak can be attributed to the release of adsorbed H_2S on the pipeline following the intersection of the by-pass and reactor lines. Previous studies also reported a strong tendency of H_2S adsorption on the pipeline's wall (Wu et al., 2018).

The differences in the lowest attainable H_2S levels in fresh and spent samples indicate that the fresh sorbent with H_2 pretreatment (sample 1) present the best performance in terms of H_2S residual test, while regenerated sorbent without H_2 pretreatment (sample 3), shows the worst performance, i.e. H_2S residual level is almost 0.8 ppm higher (Fig. 5A). Fresh sorbent with no H_2 pretreatment (sample 2) also illustrates a poor performance in terms of the H_2S residual level, indicating the importance of the H_2 pretreatment step in the desulfurization experiments. The gas-phase H_2S residual concentration is generally higher for used and regenerated sorbents, which can be explained by inefficient reduction or potential textural changes due to sintering during the regeneration, pre-reduction and desulfurization. Sintering and surface morphology change are frequently noted in post desulfurization materials

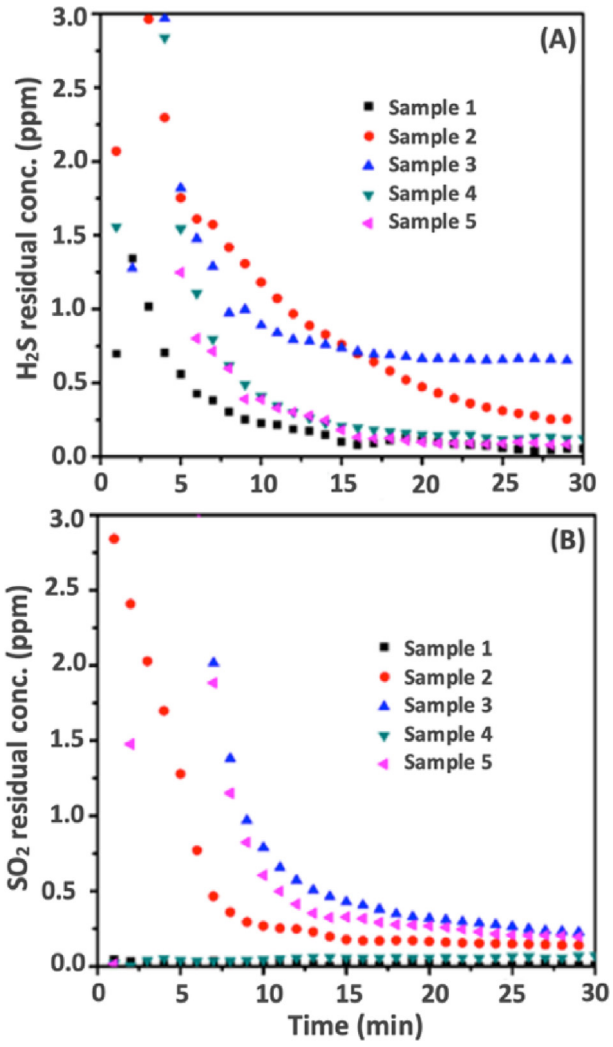

Fig. 5. Residual concentrations of (A) SO_2 and (B) H_2S in the tested samples listed in Table 2.

(Westmoreland et al., 1977; Zeng et al., 2015). Our earlier research (Ma et al., 2020) has also confirmed the textural changes and increase in the crystallite sizes in the regenerated sorbent.

The lowest attainable SO_2 level over the tested samples are presented in Fig. 5B. The residual SO_2 concentration in gas cleaned by sorbents with H_2 pretreatment (samples 1 and 4) is < 0.05 ppm through the entire sulfur residue test. However, in O_2 regenerated sorbents (i.e. samples 2, 3, and 5), the detected SO_2 level is initially high (>2 ppm), which is either from the sulfate decomposition or from the oxidation of H_2S to SO_2 in presence of higher oxidation states of metal oxides. The SO_2 level then declines to a lower level (<0.5 ppm) under reducing environment and stabilizes after 15 min. This is in agreement with the thermodynamic calculations, shown in Fig. 2.

Overall, the QMS data and the results from sulfur residue tests confirm the proposed pathways for SO_2 formation. The H_2 pre-reduction step in the O_2 –H_2 regeneration procedure seems to efficiently decompose sulfate, while reducing the oxidation states of metal oxides involved in the sulfidation experiment. As a result, the SO_2 formation in the consequent sorption cycle is prevented. Therefore, the new regeneration method (O_2–H_2 regeneration), provides a better performance than O_2 regeneration alone.

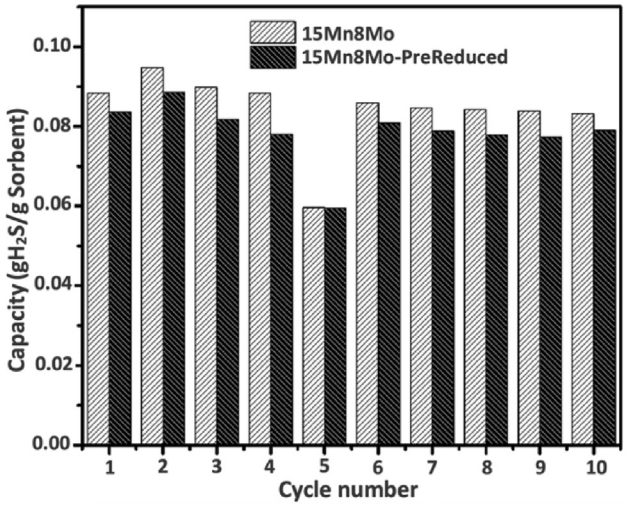

Fig. 6. Sorbent capacity in samples regenerated with and without H_2 prereduction step.

3.5. Effects of H_2 pre-reduction on the sorbent capacity and stability

To evaluate the role of H_2 pretreatment on the capacity and stability of sorbents during the chemical looping desulfurization experiments, two different performance tests with and without H_2 pretreatment following O_2 regeneration were conducted. As shown in Fig. 6, sorption capacities for the sorbents going through an extra reduction step are slightly lower (~6 %) than that without pre-reduction steps. However, both sorbents maintain a good stability, maintaining approx. 90 % of the capacity throughout 10 repeated sorption-regeneration cycles, except for the 5th cycle, which was conducted after overnight storage of the sample. The results demonstrate that the sorbent regenerated by the O_2–H_2 procedure retain good desulfurization stability, with only a slight decrease (<6 %) in overall capacity.

4. Conclusion

The impact of the regeneration conditions on the active species of the 15Mn8Mo/Al_2O_3 sorbent was investigated both experimentally and using thermodynamic calculations. Regeneration at high temperature and higher O_2 concentrations were found to be necessary to completely eliminate sulfide-based species on the spent sorbent. To counter the formation of less active species with high oxidation states (i.e., Mn_2O_3 and MoO_3), a novel O_2-H_2 regeneration step was implemented. This step removes sulfates and reduces the presence of high oxidation state species which otherwise leads to the formation of SO_2 in the subsequent sorption experiment. Furthermore, the novel O_2 –H_2 regeneration approach was tested in repeated desulfurization experiments for 10 continuous cycles. The treatment gave a slight drop in the overall capacity, but the formation of SO_2 during the initial stage of sorption was eliminated and the residual sulfur concentration in the gas phase was much lower compared to the regular O_2–regeneration method. Overall, the current study sheds light on the most efficient regeneration conditions for the performance of Mn-based solid sorbents in the high-temperature desulfurization of syngas from biomass gasification.

CRediT authorship contribution statement

Jianyu Ma: Conceptualization, Methodology, Investigation, Visualization, Data curation, Writing - original draft. **Mehdi Mahmoodinia:** Validation, Methodology, Data curation, Writing – review & editing. **Kumar R. Rout:** Supervision, Writing – review & editing, Funding acquisition, Resources. **Edd A. Blekkan:** Supervision, Writing – review & editing, Project administration, Funding acquisition.

Data availability

Data will be made available on request.

Declaration of Competing Interest

The authors declare that they have no known competing financial interests or personal relationships that could have appeared to influence the work reported in this paper.

Acknowledgements

The authors are grateful for financial support from The Norwegian Research Council through contract no. 267986.

Appendix A. Supplementary material

Supplementary data to this article can be found online at https://doi.org/10.1016/j.ces.2023.118674.

References

Abdoulmoumine, N., Adhikari, S., Kulkarni, A., Chattanathan, S., 2015. A review on biomass gasification syngas cleanup. Appl. Energy. 155, 294–307. https://doi.org/10.1016/j.apenergy.2015.05.095.

Asaoka, S., Hayakawa, S., Kim, K.H., Takeda, K., Katayama, M., Yamamoto, T., 2012. Combined adsorption and oxidation mechanisms of hydrogen sulfide on granulated coal ash. J. Colloid Interface Sci. 377, 284–290. https://doi.org/10.1016/j.jcis.2012.03.023.

Bakker, W.J.W., Kapteijn, F., Moulijn, J.A., 2003. A high capacity manganese-based sorbent for regenerative high temperature desulfurization with direct sulfur production. Chem. Eng. J. 96, 223–235. https://doi.org/10.1016/j.cej.2003.08.022.

Bale, C.W., Bélisle, E., Chartrand, P., Decterov, S.A., Eriksson, G., Gheribi, A.E., Hack, K., Jung, I.H., Kang, Y.B., Melançon, J., Pelton, A.D., Petersen, S., Robelin, C., Sangster, J., Spencer, P., Van Ende, M.A., 2016. FactSage thermochemical software and databases, 2010–2016. Calphad. 54, 35–53. https://doi.org/10.1016/J.CALPHAD.2016.05.002.

Ben-Slimane, R., Hepworth, M.T., 1994. Desulfurization of hot coal-derived fuel gases with manganese-based regenerable sorbents. 1. Loading (Sulfidation) Tests. Energy & Fuels. 8, 1175–1183. https://doi.org/10.1021/ef00048a003.

Biesinger, M.C., Payne, B.P., Grosvenor, A.P., Lau, L.W.M.W., Gerson, A.R., Smart, R.S. C., 2011. Resolving surface chemical states in XPS analysis of first row transition metals, oxides and hydroxides: Cr, Mn, Fe, Co and Ni. Appl. Surf. Sci. 257, 2717–2730. https://doi.org/10.1016/j.apsusc.2010.10.051.

Cheah, S., Carpenter, D.L., Magrini-Bair, K.A., 2009. Review of mid- to high-temperature sulfur sorbents for desulfurization of biomass- and coal-derived syngas. Energy and Fuels. 23, 5291–5307. https://doi.org/10.1021/ef900714q.

Chytil, S., Kure, M., Lødeng, R., Blekkan, E.A., 2017. Performance of Mn-based H_2S sorbents in dry, reducing atmosphere – Manganese oxide support effects. Fuel. 196, 124–133. https://doi.org/10.1016/j.fuel.2017.01.087.

Davydov, A.A., Marshneva, V.I., Shepotko, M.L., 2003. Metal oxides in hydrogen sulfide oxidation by oxygen and sulfur dioxide: I. The comparison study of the catalytic activity. Mechanism of the interactions between H_2S and SO_2 on some oxides. Appl. Catal. A Gen. 244, 93–100. https://doi.org/10.1016/S0926-860X(02)00573-2.

Di Castro, V., Polzonetti, G., 1989. XPS study of MnO oxidation. J. Electron Spectros. Relat. Phenomena. 48, 117–123. https://doi.org/10.1016/0368-2048(89)80009-X.

Gasper-Galvin, L.D., Atimtay, A.T., Gupta, R.P., 1998. Zeolite-supported metal oxide sorbents for hot-gas desulfurization. Ind. Eng. Chem. Res. 37, 4157–4166. https://doi.org/10.1021/ie930439i.

Hepworth, B.-S.-T., 1994. Desulfurization of hot coal-derived fuel gases with manganese-based regenerable sorbents. 2. regeneration and multicycle tests. Energy Fuels 8 (6), 1184–1191. https://doi.org/10.1021/ef00048a004.

Herszage, J.N., Dos, M., Afonso, S., 2003. Mechanism of Hydrogen Sulfide Oxidation by Manganese(IV) Oxide in Aqueous Solutions. Langmuir 19 (23), 9684–9692. https://doi.org/10.1021/la034016p.

Huber, G.W., Iborra, S., Corma, A., 2006. Synthesis of transportation fuels from biomass: chemistry, catalysts, and engineering. Chem. Rev. 106, 4044–4098. https://doi.org/10.1021/cr068360d.

Karayilan, D., Dogu, T., Yasyerli, S., Dogu, G., 2005. Mn−Cu and Mn−Cu−V Mixed-Oxide Regenerable Sorbents for Hot Gas Desulfurization. Ind. Eng. Chem. Res. 44, 5221–5226. https://doi.org/10.1021/ie0492496.

Lillebø, A.H., Holmen, A., Enger, B.C., Blekkan, E.A., 2013. Fischer-Tropsch conversion of biomass-derived synthesis gas to liquid fuels, Wiley Interdiscip. Rev. Energy Environ. 2, 507–524. https://doi.org/10.1002/wene.69.

Liu, L.P., Ju, S.G., Wang, H.Q., Zhao, X.W., Mi, J., 2016. Characteristics and regeneration properties of manganese oxide sorbent under O_2 atmosphere. Mater. Sci. Forum 859, 134–139. https://doi.org/10.4028/www.scientific.net/MSF.859.134.

Ma, J., Rout, K.R., Sauer, M., Mahmoodinia, M., Blekkan, E.A., 2020. Investigations of molybdenum-promoted manganese-based solid sorbents for H_2S capture. Biomass and Bioenergy 143,. https://doi.org/10.1016/j.biombioe.2020.105843 105843.

Ma, J., Mahmoodinia, M., Rout, K.R., Blekkan, E.A., 2021. Regenerable Sorbents for High-Temperature Desulfurization of Syngas from Biomass Gasification. Chemie-Ingenieur-Technik. 93, 949–958. https://doi.org/10.1002/cite.202000217.

Meng, X., De Jong, W., Pal, R., Verkooijen, A.H.M., 2010. In bed and downstream hot gas during solid fuel gasification: a review. Fuel Process. Technol. 91, 964–981. https://doi.org/10.1016/j.fuproc.2010.02.005.

Oku, M., Hirokawa, K., Ikeda, S., 1975. X-ray photoelectron spectroscopy of manganese-oxygen systems. J. Electron Spectros. Relat. Phenomena. 7, 465–473. https://doi.org/10.1016/0368-2048(75)85010-9.

Pishahang, M., Larring, Y., Van Dijk, E., Van Berkel, F., Dahl, P.I., Cobden, P., McCann, M., Bakken, E., 2016. Regenerative Copper-Alumina H_2S Sorbent for Hot Gas Cleaning through Chemical Swing Adsorption. Ind. Eng. Chem. Res. 55, 1024–1032. https://doi.org/10.1021/acs.iecr.5b03752.

Sjoerd Kijlstra, W., Biervliet, M., Poels, E.K., Bliek, A., 1998. Deactivation by SO_2 of MnO_x/Al_2O_3 catalysts used for the selective catalytic reduction of NO with NH_3 at low temperatures. Appl. Catal. B Environ. 16, 327–337. https://doi.org/10.1016/S0926-3373(97)00089-1.

Wang, H., Shangguan, J., Liu, L., Zhao, X., Mi, J., 2016. The Regeneration properties of Manganese Oxide Sorbent under SO_2 Atmosphere. Mater. Sci. Forum 859, 140–145. https://doi.org/10.4028/www.scientific.net/MSF.859.140.

Westmoreland, P.R., Harrison, D.P., 1976. Evaluation of candidate solids for high-temperature desulfurization of low-btu gases. Environ. Sci. Technol. 10, 659–661. https://doi.org/10.1021/es60118a010.

Westmoreland, P.R., Gibson, J.B., Harrison, D.P., 1977. Comparative Kinetics of High-Temperature Reaction Between H_2S and Selected Metal Oxides. Environ. Sci. Technol. 11 (5), 488–491. https://doi.org/10.1021/es60128a007.

Woolcock, P.J., Brown, R.C., 2013. A review of cleaning technologies for biomass-derived syngas. Biomass and Bioenergy 52, 54–84. https://doi.org/10.1016/J.BIOMBIOE.2013.02.036.

Wu, J., Liu, D., Zhou, W., Liu, Q., Huang, Y., 2018. High-Temperature H_2S Removal from IGCC Coarse Gas, Springer Singapore. Singapore. https://doi.org/10.1007/978-981-10-6817-1.

Xuan, Y., Yu, Q., Qin, Q., Wang, K., Duan, W., Liu, K., Zhang, P., 2018. Selection of Desulfurizer and Control of Reaction Products on Flue-Gas Desulfurization Using Chemical-Looping Technology. Energy Fuels 32 (1), 889–900. https://doi.org/10.1021/acs.energyfuels.7b03117.

Xuan, Y., Yu, Q., Wang, K., Duan, W., Li, Y., Qin, Q., Xue, Z., 2020. Evaluation of Mn-based sorbent for flue gas desulfurization through isothermal chemical-looping system. Chem. Eng. J. 379. https://doi.org/10.1016/j.cej.2019.122283.

Yasyerli, S., 2008. Cerium-manganese mixed oxides for high temperature H_2S removal and activity comparisons with V-Mn, Zn-Mn, Fe-Mn sorbents. Chem. Eng. Process. Process Intensif. 47, 577–584. https://doi.org/10.1016/j.cep.2006.11.016.

Yu, J., Chang, L., Li, F., Xie, K., 2010. A review on research and development of iron-based sorbents for removal of hydrogen sulfide from hot coal gases. Front. Chem. Eng. China. 4, 529–535. https://doi.org/10.1007/s11705-010-0519-4.

Zeng, B., Li, H., Huang, T., Liu, C., Yue, H., Liang, B., 2015. Kinetic study on the sulfidation and regeneration of manganese-based regenerable sorbent for high temperature H_2S removal. Ind. Eng. Chem. Res. 54, 1179–1188. https://doi.org/10.1021/ie503233a.

Zeng, Y., Zhang, S., Groves, F.R., Harrison, D.P., 1999. High temperature gas desulfurization with elemental sulfur production. Chem. Eng. Sci. 54, 3007–3017. https://doi.org/10.1016/S0009-2509(98)00427-8.

Zhang, J., Wang, Y., Wu, D., 2003. Effect investigation of ZnO additive on Mn-Fe/γ-Al_2O_3 sorbents for hot gas desulfurization. Energy Convers. Manag. 44, 357–367. https://doi.org/10.1016/S0196-8904(02)00068-7.